Imaging, Diagnosis, Prognosis

Clinical Cancer Research

Metabolic Imaging: A Link between Lactate Dehydrogenase A, Lactate, and Tumor Phenotype

Inna Serganova[1], Asif Rizwan[2], Xiaohui Ni[2], Sunitha B. Thakur[2,3], Jelena Vider[1], James Russell[2], Ronald Blasberg[1,3,5], and Jason A. Koutcher[2,3,4,5]

Abstract

Purpose: We compared the metabolic profiles and the association between LDH-A expression and lactate production in two isogenic murine breast cancer cell lines and tumors (67NR and 4T1). These cell lines were derived from a single mammary tumor and have different growth and metabolic phenotypes.

Experimental Design: LDH-A expression, lactate concentration, glucose utilization, and oxygen consumption were measured in cells, and the potential relationship between tumor lactate levels [measured by magnetic resonance spectroscopic imaging (MRSI)] and tumor glucose utilization [measured by [^{18}F]2-deoxy-2-fluoro-D-glucose positron emission tomography ([^{18}F]FDG-PET)] was assessed in orthotopic breast tumors derived from these cell lines.

Results: We show a substantial difference in LDH-A expression between 67NR and 4T1 cells under normoxia and hypoxia. We also show that small orthotopic 4T1 tumors generate 10-fold more lactate than corresponding 67NR tumors. The high lactate levels in small primary 4T1 tumors are associated with intense pimonidazole staining (a hypoxia indicator). Less-intense hypoxia staining was observed in the larger 67NR tumors and is consistent with the gradual increase and plateau of lactate concentration in enlarging 67NR tumors.

Conclusions: Lactate-MRSI has a greater dynamic range than [^{18}F]FDG-PET and may be a more sensitive measure with which to evaluate the aggressive and metastatic potential of primary breast tumors. *Clin Cancer Res; 17(19); 6250–61. ©2011 AACR.*

Introduction

Metabolic changes in primary tumors have a significant impact on tumor progression and on the development of the metastatic phenotype (1, 2). The accumulation of lactate in tumor cells was first described by Warburg and is associated with aerobic glycolysis (3). Clinical studies showed that high lactate levels (with median concentrations >8 mmol/L) are associated with the subsequent development of metastases (4) and include primary cervical, head and neck, and rectal cancers (5–7). The recent coupling between metabolic and genetic variations in cancer cells has stimulated renewed interest in the role of cellular metabolism (2, 8, 9). In cancer patients, serum total lactate dehydrogenase (LDH) levels are often increased, and the gene for *LDH-A* protein is often upregulated in tumors (10, 11). These features have been linked to poor prognosis (11–15), and a greater metastatic potential has been reported in patients with high LDH serum levels (11, 14). Because LDH-A protein is required for the maintenance and progression of many tumors (10, 16), it is also becoming a potential target for cancer therapy (16–18). Many cancers, particularly those originating in the breast and ovary, are highly heterogeneous, representing a large array of diseases with different etiologies (19) and with distinct genetic and phenotypic signatures (20). The metabolic response of individual tumor cells within a tumor is dependent on the environmental conditions (nutrient depletion, hypoxia, acidity, specific stromal cell components, etc.) encountered within the local tumor microenvironment, as well as specific oncogenic and/or tumor suppressor mutations of the tumor cell itself (9).

We investigated the relationship between LDH-A expression and lactate production in 2 isogenic breast cancer lines (67NR and 4T1). These 2 cell lines were derived from a single mammary tumor that developed spontaneously in a BALB/c mouse. Each subclone was shown to have different phenotypic properties (21–23). 67NR cells form primary tumors but do not metastasize. 4T1 cells are able to

Authors' Affiliations: Departments of [1]Neurology, [2]Medical Physics, [3]Radiology, and [4]Medicine, [5]Molecular Pharmacology and Chemistry Program, Memorial Sloan Kettering Cancer Center, New York, New York

Note: Supplementary data for this article are available at Clinical Cancer Research Online (http://clincancerres.aacrjournals.org/).

I. Serganova, A. Rizwan, and X. Ni contributed equally to this work.

Corresponding Author: Jason A. Koutcher, Imaging and Spectroscopic Physics, Department of Medical Physics, Genitourinary Oncology Medicine, Memorial Sloan Kettering Cancer Center, Room MRI 1125, 1275 York Avenue, New York, NY 10021. Phone: 212-639-8834; Fax: 212-717-3676; E-mail: koutchej@mskcc.org

doi: 10.1158/1078-0432.CCR-11-0397

Translational Relevance

Using subclones derived from a single spontaneous murine breast tumor, we show that the more aggressive clone (4T1, with a high propensity to metastasize to lung and other organs) produces higher levels of lactate in small tumors that are associated with higher *LDH-A* expression and a higher intensity of pimonidazole staining, when compared with the nonmetastatic 67NR clone. Lactate-MRSI, but not [^{18}F]2-deoxy-2-fluoro-D-glucose positron emission tomography ([^{18}F]FDG-PET) imaging, was able to identify significant differences in the metabolic phenotype between these 2 orthotopic tumors. There was a 10-fold higher level of lactate in small 4T1 tumors than in 67NR tumors, at the time 4T1 lung metastases were developing. In contrast, there was only a 1.1-fold difference in [^{18}F]FDG accumulation in the same tumors. These studies show a much greater dynamic range for tumor lactate measurements than for measurements of [^{18}F]FDG accumulation in these tumor models.

complete all steps leading to distant metastases and efficiently form macroscopic nodules in the lung (21) and other organs (22, 24). We have shown a substantial variation in LDH-A expression between these 2 cell lines under normoxia and hypoxia that reflect LDH enzyme activity and lactate concentrations in tumors. Consistent with other reports (25, 26), only minor changes in LDH-B expression were observed. We also studied the potential correlation between glucose utilization, as measured by [^{18}F]2-deoxy-2-fluoro-D-glucose uptake and positron emission tomography ([^{18}F]FDG-PET), and lactate production, as measured by magnetic resonance spectroscopic imaging (MRSI), in growing orthotopic tumors.

We consider LDH to be a critical branch point in metabolism. It is involved in the metabolism of the 2 major nutrients, glucose and glutamine, as well as in determining tumor pH and the activity of the tricarboxylic acid (TCA) cycle (27). We hypothesized that tumor lactate levels monitored by MRSI will reflect LDH-A enzymatic activity and tumor phenotype. We show that lactate-MRSI measurements have a greater dynamic range than concurrent [^{18}F]FDG-PET measurements. We suggest that lactate-MRSI is a more sensitive measure than [^{18}F]FDG-PET and could be used in the clinic to evaluate the aggressive potential of primary breast tumors, as this imaging technology has been applied in human tumors.

Materials and Methods

Cell culture and growth

Two isogenic tumorigenic cell lines (67NR and 4T1), derived from a spontaneous breast tumor in a BALB/c mouse (provided by Fred Miller; Karmanos Cancer Institute, Detroit, MI), were studied. Cells were grown in complete Dulbecco's Modified Eagle's Media containing 10% fetal calf serum with 2 mmol/L L-glutamine and penicillin/streptomycin. Cells were plated at a density of 5×10^6 cells. Fourteen hours later, plates were placed under normal or hypoxic (1%) conditions to assess cell growth. During days 2 to 6, cells were trypsinized and resuspended in 1 mL of medium. Cells were counted using Countess Automated Cell Counter (Invitrogen).

Assessment of *LDH-A* mRNA expression

For all mRNA and proteins assays, we used cells growing for 48 hours (exponential growth phase). RNA was isolated using an "RNeasy" total RNA isolation kit (Qiagen), following the manufacturer's protocol. The presence of LDH-A and β-actin mRNAs was assessed using a QIAGEN One-Step RT-PCR kit. The mouse LDH-A cDNAs were amplified using the oligonucleotides 5′-CCTGTGGCTGGGCTCTTGG C-3′ and 5′-AGCCGGCTCTCCCCCTCTTG-3′. The level of β-actin transcript was used as an internal control and amplified using the oligonucleotides 5′-CCTAAGGC-CAACCGTGAAAAGATG-3′ and 5′-GGGTGTAAACGCAGC TCAGTAAC-3′.

Western blotting

Breast cancer cell pellets underwent protein extraction using RIPA Buffer (25 mmol/L Tris HCl, pH = 7.6, 150 mmol/L NaCl, 1% NP-40, 1% sodium deoxycholate, 0.1% SDS; Thermo Scientific) and protease inhibitors cocktail (1:100; Thermo Scientific Halt Protease Inhibitor Cocktail). Protein concentrations were determined with bicinchoninic acid assay (BCA Protein Assay Kit; Pierce). In equivalent amounts (5–20 μg per well), the proteins were separated by electrophoresis using a NuPAGE 4-12% Bis-Tris gradient gel (Invitrogen) and transferred to an Immun-Blot PVDF membrane (BioRad). Membranes were blocked in 5% milk in TBS with Tween-20 buffer and were immunoblotted with anti-LDH-A antibody (#2012; Cell Signaling Technology) at a 1:1,000 dilution, anti-HXKII antibody (c-14, sc-6521; Santa Cruz Biotechnology) at a 1:200 dilution, anti-PKM2 antibody (#3198; Cell Signaling Technology) at a 1:1,000 dilution, and anti-LDH-B antibody (#1974-1; Epitomics) at a 1:1,000 dilution. Bound primary antibodies were visualized with appropriate horseradish peroxidase–conjugated secondary antibodies (1:2,000) using enhanced chemiluminescence reagent (Western Lightning-ECL). Immunoblots were stripped using Restore Western Blot Stripping Buffer (Thermo Scientific) and reprobed with anti-β-actin antibody (Abcam) at a 1:5,000 dilution.

LDH activity

Total LDH activity of 67NR and 4T1 cells was assessed using the Cytotoxicity Detection Kit PLUS (LDH; Roche Diagnostics). Different numbers of cells were plated in 96-well plates and incubated (37°C, 5%CO_2, 90% humidity) for 3 to 6 hours and lysed, and LDH activity was measured as described by the manufacturer.

Glucose utilization

Glucose utilization of 67NR and 4T1 cells was assessed using the Glucose Assay Kit (MBL International). The glucose concentration in growth medium was measured and compared with a control medium at days 2 and 5.

L-Lactate

Lactate production by 67NR and 4T1 cells during growth was assessed by measuring the culture medium lactate using an L-lactate assay kit (Eton Bioscience).

Oxygen consumption assay

Oxygen consumption was measured using the OxyLite system (Oxford Optronics; ref. 28). Cells were cultured in 75 cm^2 flasks to approximately 90% confluence. Cells were trypsinized to prepare single cells in the growth media containing 25 mmol/L HEPES. Cells were suspended in 5 mL medium and incubated in sealed Reacti-vials (Pierce Scientific, now known as Thermo Fisher Scientific Inc.) at 37°C, with continuous stirring. The OxyLite probe was introduced into the cell mix using a 19-G needle to pierce the rubber septum. Measurements were recorded over 30 to 60 minutes. Medium pH was measured before and after the experiment. To show a maximal inhibition of the electron transfer chain, an inhibitor of the respiratory chain, rotenone was added to cells for 30 minutes at concentrations of 1 or 10 μmol/L. All experiments were repeated at least 3 times with cells from independent cultures.

Animal model

The animal protocol was approved by the Institutional Animal Care and Use Committee of Memorial Sloan Kettering Cancer Center. A total of 1×10^6 67NR and 4T1 cells were injected into the fourth right mammary fat pad of athymic *nu/nu* female mice (National Cancer Institute). Tumors were categorized into following 3 groups: small (<150 mm^3), medium (150–400 mm^3), and large (>400 mm^3). Tumor volume (V) was calculated from caliper measurements, where $V = (\pi/6) \times x \times y \times z$ where x, y, and z are 3 orthogonal diameters. A total of 20 mice [67NR ($n = 8$) and 4T1 ($n = 12$)] were used in the imaging experiments.

In vivo lactate detection

The lactate level in the tumor was detected using MRSI. Tumor-bearing mice were anesthetized with isoflurane (1.5%) combined with oxygen. MRSI experiments were carried out on a 7T Bruker Biospec Spectrometer using home-built 2-turn solenoid coils (7 and 12 mm in diameters). The coil was positioned in the center of the platform and matched with the isocenter of the magnet. Scout images acquired with the Bruker ParaVision TriPilot Sequence ensured that the tumor was in the center of the magnet. The body temperature of the mice was monitored and maintained at 35°C using a rectal temperature probe and warm air was directed on the animal (MR-compatible, small rodent Heater System; SA Instruments). The lactate signal was detected using the Selective Multiple Quantum Coherence (SelMQC) editing sequence (29, 30). Spectra of both the whole tumor and a 5-mm thick center slice in the coronal plane were acquired with repetition time (TR) = 2 seconds, number of excitations = 8,512 data points, and spectral width = 2,510 Hz. Two-dimensional chemical shift imaging (2D-CSI) of the localized, 5-mm thick coronal slice was conducted with the following parameters: matrix size = 16 × 16 and field of view = 24 mm (1.5 × 1.5 mm^2 in plane resolution). The voxel volume of the CSI was 11.25 mm^3, and total 2D-CSI acquisition time was 70 minutes. The 2D-CSI was coregistered with a T_2-weighted image using a multislice multiecho sequence (MSME). The parameters for the MSME included a slice thickness = 1 mm, field of view = 24 mm, 2,217-ms repetition time, 40-ms echo time, matrix size = 512 × 256, and number of average = 8. Multislice images of the tumor in the coronal plane were also acquired using rapid acquisition with relaxation enhancement (RARE) sequence with a slice thickness of 1 mm. The volumes of the tumor in the central slice for CSI were calculated by drawing regions of interest (ROI) in the T_2-weighted image to find the tumor area and then multiplying the area by the slice thickness.

Magnetic resonance data processing

The 1D lactate spectra from the 5-mm thick center slice were processed by a 1D Fourier transform, similar to our previous methodology (31). The absolute magnitude of the echo signal from the slice was fitted by a home-written program using Matlab (The MathWorks) and normalized to the slice volume. Lactate spectra quantitation was conducted by the phantom replacement technique (32), using a 10 mmol/L lactate/H_2O cylinder. The concentration of *in vivo* tumor lactate, C, can be calculated from the phantom solution of known lactate concentration C^{ref} as follows:

$$C = C^{ref} \times f_{T_1,T_2} \times \frac{A}{A^{ref}}$$

where A and A^{ref} are the measured areas under the fitted peaks in tumor and in the reference phantom, respectively. The relaxation times, T_1 and T_2, were measured using modified T_1-SelMQC and T_2-SelMQC sequences which have been described elsewhere (30). The correction factor for T_1 and T_2 differences between phantom and *in vivo* data is as follows:

$$f_{T_1,T_2} = \exp\left[TE\left(\frac{1}{T_{2\,vivo}} - \frac{1}{T_{2\,phantom}}\right)\right] \times \frac{\left[1-\exp\left(-TR/T_{1\,phantom}\right)\right]}{\left[1-\exp\left(-TR/T_{1\,vivo}\right)\right]}$$

The T_1 values for the 67NR and 4T1 are 1.61 and 1.86 seconds, respectively. The T_2 values for the 67NR and 4T1 tumors are 0.21 and 0.34 seconds, respectively. For the lactate phantom, the T_1 is 1.3 seconds and T_2 is 0.5 seconds. The 2D-CSI data from the tumor and the phantom were processed voxel by voxel by the 3DiCSI Software Package (courtesy of Truman Brown, PhD, Columbia University, New York, NY). The spectra from the 2D-CSI were superimposed on the corresponding T_2-weighted MSME image

using the 3DiCSI software. The spectrum from each tumor voxel was extracted for further processing by software written using Matlab. Voxel volume was selected as 11.25 mm^3 for both tumor and phantom. Also, the maximum concentration of lactate in a voxel was identified (hot spot for lactate) and recorded.

MicroPET

[^{18}F]FDG-PET imaging was conducted after lactate-MRSI, as previously described (33). [^{18}F]FDG (specific activity > 11 Ci/mmol, average purity 99%) was provided by IBA Molecular. An experimentally determined system calibration factor was used to convert voxel count rate to radioactivity concentrations, expressed as percentage of injected dose/mL (%ID/mL). ROI analysis of the reconstructed images was conducted using ASIPro software (Siemens Medical Solutions) to determine the average and maximum tumor radioactivity values. A partial volume correction was applied to the ROI-measured radioactivity data (Supplementary Fig. S1).

Immunohistochemical staining

Selected animals were injected with pimonidazole hydrochloride (hypoxyprobe-1, HPI) and Hoechst 33342 (Sigma-Aldrich) at 60 and 40 mg/kg, respectively. These agents were dissolved in PBS and administered by way of the tail vein. Pimonidazole hydrochloride was administered 1 hour presacrifice, and Hoechst 33342 was administered 5 minutes presacrifice (34). Tumors were immediately frozen at −80°C for immunohistochemistry. Ten-micrometer thick, adjacent frozen sections from the estimated location of the MRS slice were obtained using a Microm HM500 cryostat microtome (Microm International GmbH). The sections were imaged for Hoechst (blood perfusion) and for pimonidazole (hypoxia) detection. The sections were then stained with CD31 antibody (endothelial cell marker), and adjacent tumor sections were processed for hematoxylin and eosin (H&E) staining. Images of the sections were processed using Matlab to estimate the fraction of tumor necrosis (31).

Statistical analyses

All values are expressed as mean ± SD. Statistical significance was determined by a 2-tailed Student's *t* test; a value of $P < 0.05$ was considered significant.

Results

Metabolic characterization of 67NR and 4T1 murine breast cancer cell lines

The metabolic features of 2 isogenic tumor cell lines, with different phenotypic growth and metastatic characteristics, were compared and related to LDH-A mRNA expression and protein levels. Semiquantitative reverse transcriptase (RT)-PCR and immunoblotting for LDH-A showed that nonmetastatic 67NR cells express lower levels of LDH-A in comparison with highly aggressive, metastases prone 4T1 cells during exponential growth under normal incubation conditions (Fig. 1A and B). To confirm that LDH-A expression levels correlate with the functional activity of LDH as an enzymatic complex, we conducted an enzymatic assay in viable 67NR and 4T1 cancer cells (Fig. 1C). LDH activity was approximately 5-fold higher in 4T1 cells than in 67NR cells.

We also assessed the expression levels of 2 other glycolytic enzymes, HXKII (hexokinase II) and PKM2 (pyruvate kinase muscle isozyme 2; Fig. 1B). HXKII and PKM2 are overexpressed in 4T1 cells compared with 67NR cells; the relative intensity of the immunoblot bands was measured and showed a 3- and 2-fold difference, respectively (data not shown).

A significant difference in acidification of the incubation medium and lactate production was also observed between the 2 cell lines (Fig. 1D and G). At day 5 of cell growth, the medium pH of 4T1 was 6.9 ± 0.1 whereas the medium pH of 67NR cells was 7.4 ± 0.1. Glucose utilization by 67NR and 4T1 cells was also significantly different (Fig. 1F); 4T1 cells exhausted the supply of glucose in the medium within 5 days of incubation whereas 67NR cells used only 50% of the available glucose during this period. These differences are significant at day 5 of cell growth and cannot be explained by differences in cell numbers.

Many advanced cancers that reflect the Warburg phenotype have high glucose uptake with conversion of glucose to lactate. Cells with this phenotype consume available oxygen at a rate dictated by their oxidative capacity, and this consumption rate can be measured. Interestingly, 4T1 cells had a 3-fold higher rate of oxygen consumption than 67NR cells. The inhibition of the mitochondrial respiratory chain complex I by 1 μmol/L rotenone was approximately 90% in 4T1 cells and 100% in 67NR cells (Fig. 1E). Rotenone at 10 μmol/L completely inhibited oxygen consumption in both cell lines.

In vivo lactate detection with ^{1}H-MRSI using a SelMQC sequence

Because 67NR and 4T1 cancer cells show significant differences in the expression of HXKII, PKM2, and LDH-A, as well as glycolytic flux and mitochondrial respiration, we decided to assess whether they exhibited a different metabolic phenotype *in vivo* as well. Lactate concentration in 67NR and 4T1 tumors was monitored by MRSI using the SelMQC sequence during tumor growth (the tumor growth profiles are shown in Supplementary Fig. S2). The 2D-CSI of nonmetastatic 67NR and metastatic-prone 4T1 tumors are compared at 3 different tumor volumes (Fig. 2A and B). Note that the distribution of lactate signal varies spatially across both 67NR and 4T1 tumors, reflecting the heterogeneity of tumor metabolism. A difference in total LDH-A expression is also present in 67NR and 4T1 tumors, as assessed by Western blotting (Fig. 2C).

Small (<150 mm^3) 67NR tumors showed very low levels of lactate (average lactate = 0.9 ± 1.9 mmol/L; Fig. 3A and C). Lactate levels in 67NR tumors larger than 150 mm^3 gradually increased and reached a plateau during tumor growth, with an average concentration of

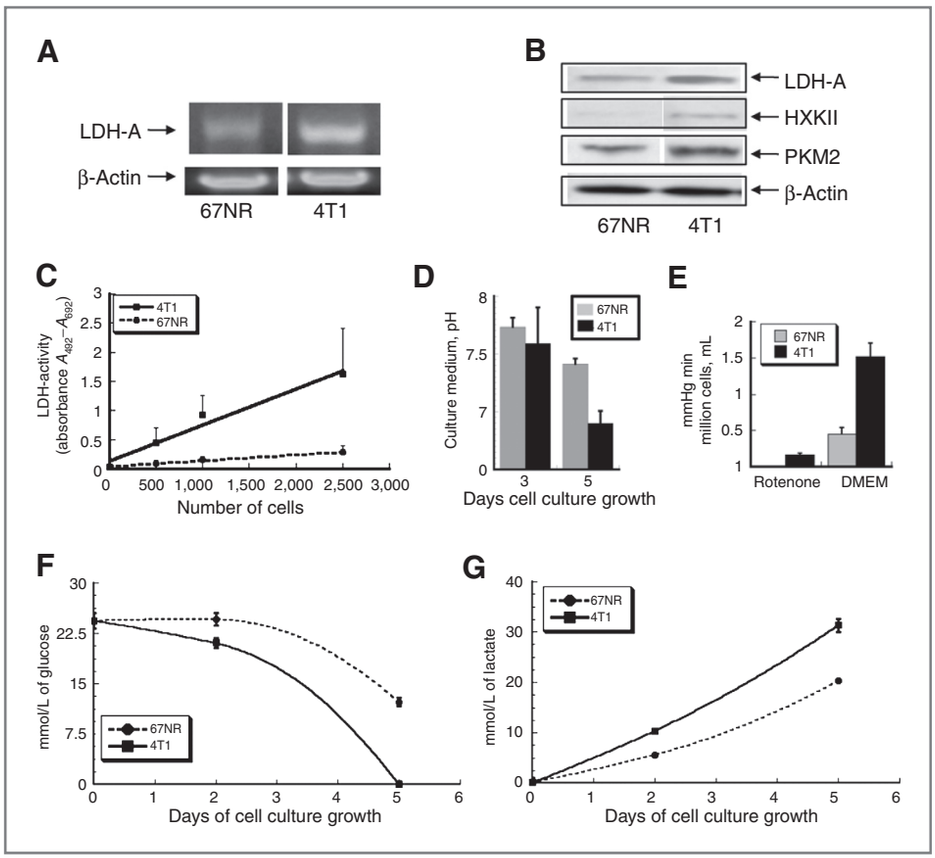

Figure 1. Metabolic features of isogenic 67NR and 4T1 breast cancer cells. A, LDH-A mRNA expression in 67NR and 4T1 cells by the semiquantitative RT-PCR. B, LDH-A, HXKII, and PKM2 proteins expression assessed by Western blotting. C, total LDH enzyme activity in 67NR cells and 4T1 cells. D, cell culture medium acidification; supernatant pH. E, oxygen consumption of 67NR and 4T1 cells in normal growth media [Dulbecco's Modified Eagle's Media (DMEM; high glucose) + 10% fetal calf serum + 2 mmol/L L-glutamine, 25 mmol/L HEPES] and upon treatment with 1 μmol/L of rotenone using the OxyLite system. F, glucose utilization; clearance of glucose from the culture medium. G, lactate production; appearance of lactate in the culture medium.

5.5 ± 1.8 mmol/L. Small (<150 mm^3) 4T1 tumors have significantly higher lactate concentrations (9.3 ± 2.7 mmol/L) than small 67NR tumors ($P = 0.0001$). In contrast to 67NR tumors, the lactate signal in 4T1 tumors decreased rapidly, as tumor size increased (Fig. 3B and C). Expressed differently, primary 4T1 tumors (6–8 days after orthotopic implantation when metastases are first detected; mean volume = 73 ± 14 mm^3) have very high lactate levels (11.0 ± 1.5 mmol/L). Plotting tumor lactate concentrations versus time after orthotopic implantation yielded lactate concentration profiles (Fig. 3D) similar to that obtained when plotted versus tumor volume (Fig. 3A and B).

An examination of the H&E sections of different size 67NR and 4T1 tumors showed that necrosis became visible in 4T1 tumors even at 100 mm^3 in size whereas necrotic areas were essentially absent in large (>400 mm^3) 67NR tumors (Supplementary Fig. S3). The decrease in lactate signal as 4T1 tumors increase in size (Fig. 3B) may be explained, in part, by the increase in tumor necrosis. We analyzed the H&E sections of 5 large 4T1 (450, 530, 670, 770, and 860 mm^3) tumors that had lactate-MRSI measurements just prior to sacrifice. The fraction of viable-appearing tissue in these large 4T1 tumors was calculated from the H&E images of these tumors using Matlab (described in Materials and Methods). When the lactate signal was corrected for the viable tissue volume, the average lactate concentration in those large 4T1 tumors was calculated to be 7.3 ± 1.4 mmol/L.

FDG microPET imaging

[^{18}F]FDG microPET scans were conducted following lactate ^{1}H-MRSI imaging on the same tumor-bearing animals. Small 67NR tumors (<150 mm^3) had an average partial volume-corrected [^{18}F]FDG uptake of 6.2 ± 1.5 %ID/mL, which slowly declined as the tumors increased in size (Fig. 4A and C). The partial volume-corrected [^{18}F]FDG uptake of small 4T1 tumors was 6.8 ± 2.2 %ID/mL, which decreased rapidly with tumor growth, approaching a plateau value of approximately 3%ID/mL as the tumors increased in size (Fig. 4B and C). All 4T1 tumors exhibited more-intense FDG accumulation along the periphery during the late stages of the growth (Fig. 4D), reflecting lower metabolism in central tumor areas with greater necrosis. MRSI also showed heterogeneity of lactate levels in medium and large 4T1 tumors, but there was not a strong segregation between the periphery and central core.

Comparison of growth profiles and LDH-A and LDH-B expression under normoxic and hypoxic conditions

4T1 cells grow more rapidly than 67NR cells during first 4 days of culture and then plateau whereas 67NR cells

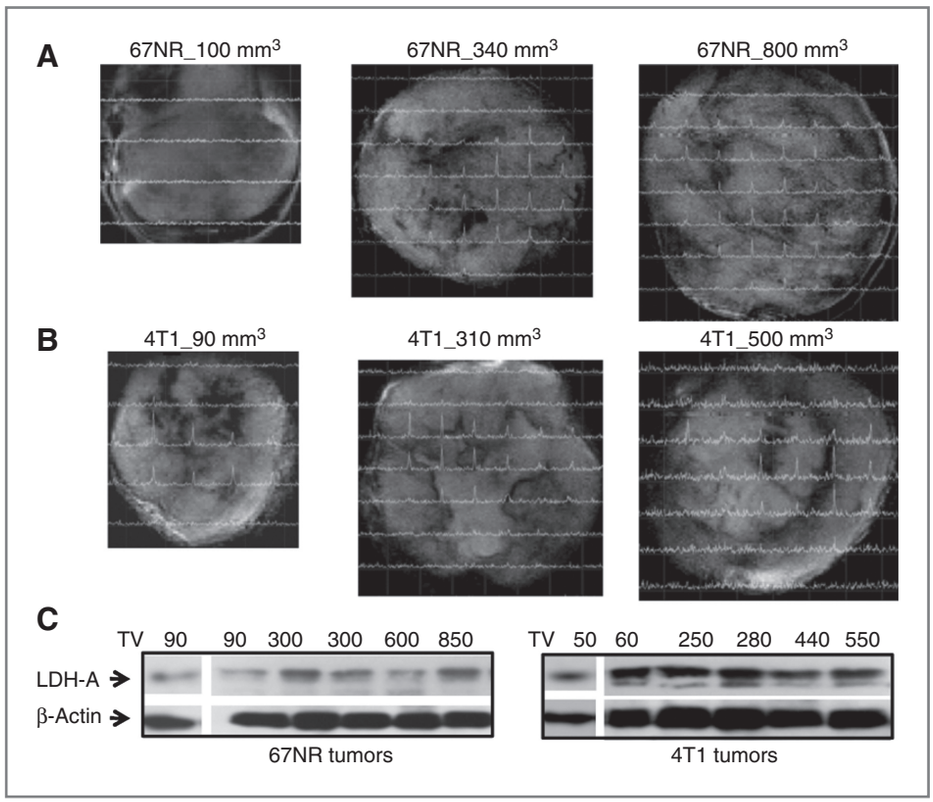

Figure 2. Lactate CSI spectra. A, different sizes of 67NR nonmetastatic tumors are shown. B, 4T1 metastasis-prone tumors are shown. Lactate signal was detected using CSI and a SelMQC editing sequence. C, LDH-A protein expression was assessed by Western blotting in different sizes of 67NR and 4T1 tumors. TV, tumor volume.

continue exponential cell growth through day 7 (Fig. 5A). Because we determined that 4T1 cells have a higher rate of oxygen consumption than 67NR cells (Fig. 1E), we conducted experiments to study the effect of hypoxia (1% oxygen) on cell growth. We found that the growth of 4T1 cells under hypoxic conditions declined after day 3 (Fig. 5A), suggesting that 4T1 cells are very sensitive to hypoxia. In contrast, 67NR cells were less affected by hypoxia and continued to grow slowly after day 3 (Fig. 5A).

We also assessed the impact of hypoxia (1% of oxygen) on LDH-A and LDH-B expression levels by immunoblotting. Hypoxia had little effect on LDH-B levels in the 2 cell lines, consistent with previous published studies (25, 26); the major change was found in LDH-A expression (Fig. 5). Importantly, 4T1 cells had a higher expression of more than 10-fold of LDH-A than 67NR cells under normoxic culture conditions, and both cell lines increase LDH-A expression in response to hypoxia (based on the β-actin–normalized intensity of the bands; Fig. 5B and C). 67NR cells have very low levels of LDH-A under normoxia, but an 18-fold upregulation was observed under hypoxia (Fig. 5B and C). Note that the LDH-A protein levels were similar in both cell lines under hypoxia.

The differential expression of LDH-A protein in 4T1 and 67NR cells under normoxic and hypoxic conditions in cell culture is consistent with the variation and difference in lactate levels measured by MRSI in small 4T1 and medium-to-large 67NR orthotopically growing tumors (Fig. 3). In support of this explanation, tumor samples were collected and processed after administration of pimonidazole hydrochloride and Hoechst 33342 (hypoxia and the blood perfusion probes, respectively; Fig. 6). Consistent with the *in vitro* results, small (100 mm^3) 4T1 tumors show small zones of necrosis (or impending necrosis) associated with pimonidazole (hypoxia) and attenuated perfusion staining. The intensity of pimonidazole staining was significantly higher in all 4T1 samples than in 67NR tumors. The visible, but less intense, hypoxia staining was observed only in the larger 67NR tumor samples. These results could partially explain the gradual increase and plateau level (5.5 ± 1.8 mmol/L) of lactate in medium and large sizes 67NR tumors as a result of increasing hypoxia that develops in the enlarging tumors (>150 mm^3; Fig. 3A). Moreover, the development of significant necrosis observed in all enlarging 4T1 tumors (Supplementary Fig. S3) may explain the lower lactate accumulation in comparison with small 4T1 tumors.

Discussion

Glucose and glutamine are the major carbon sources for rapidly proliferating tumors, providing precursors for nucleic acids, proteins, and lipids, as well as metabolic-reducing capability (NADPH). Pyruvate is largely derived from both glucose and glutamine metabolism; it can be converted to lactate by the LDH complex and/or enter the TCA cycle for conversion to CO_2 and ATP. The conversion of pyruvate to lactate is also catalyzed by LDH which is a

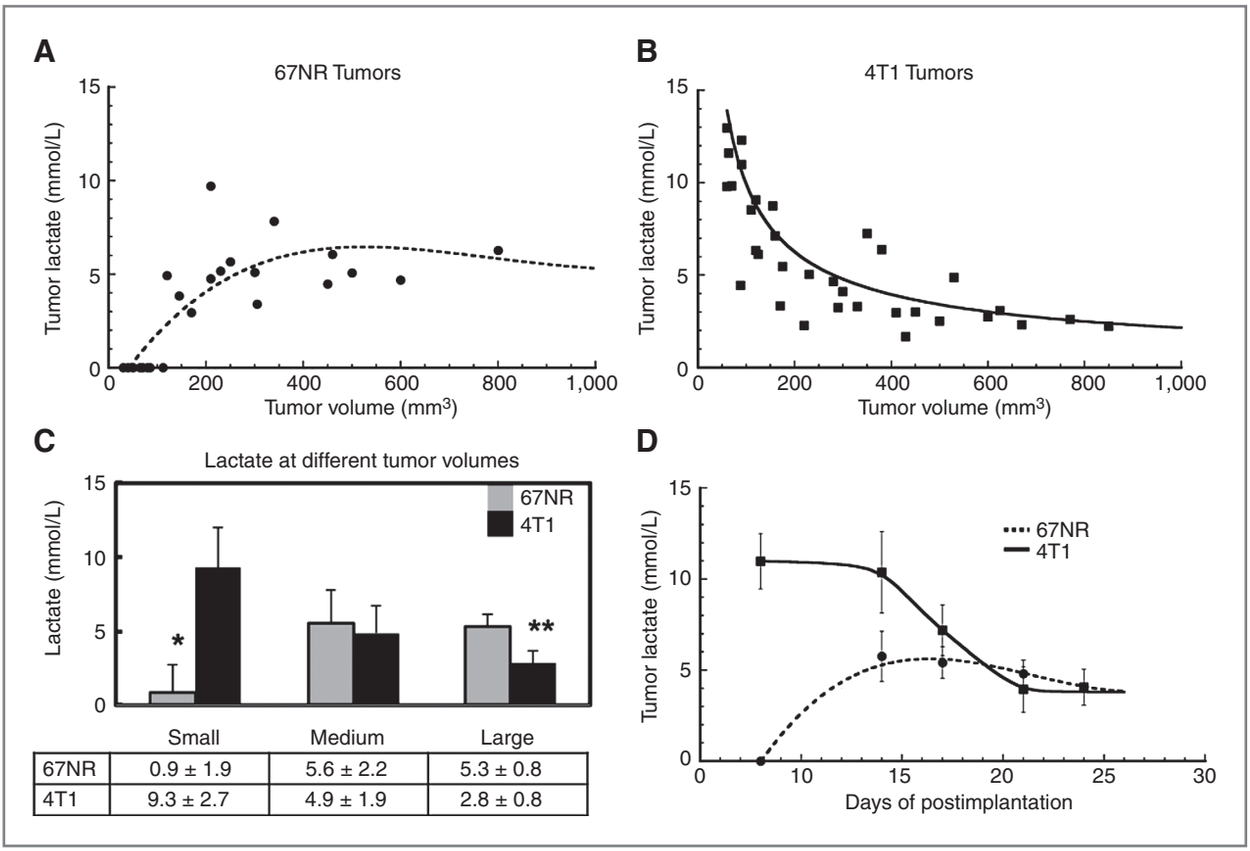

	Small	Medium	Large
67NR	0.9 ± 1.9	5.6 ± 2.2	5.3 ± 0.8
4T1	9.3 ± 2.7	4.9 ± 1.9	2.8 ± 0.8

Figure 3. MRSI measurements of lactate concentration in orthotopic 67NR and 4T1 breast tumors during tumor growth. Lactate concentration in (A) 67NR tumors (solid circles, dashed line) and in (B) 4T1 tumors (solid squares, solid line) plotted versus tumor volume. C, average lactate concentration at 3 different tumor volumes (small, <150 mm^3; medium, 150–400 mm^3; and large, >400 mm^3). Values are the mean ± SD. *, $P < 0.05$; **, $P < 0.01$. D, tumor lactate concentration plotted versus days postorthotopic implantation.

reversible reaction that results in the formation of NAD^+, which is necessary for further glycolysis. LDH isoenzymes are found in almost all eukaryotic cells and tissues, reflecting the importance of this metabolic step. As a consequence of increased glucose and glutamine metabolism, tumors secrete lactate, alanine, and NH_4^+. When oxygen is available, the accumulated and exogenous lactate can be reutilized and converted back to pyruvate, where it is further oxidized to CO_2 and H_2O in the TCA cycle, generating ATP and NAD^+ (35). Recently, it was shown that LDH-A is required for the maintenance and progression of many tumors (10, 16, 17), but the mechanisms by which LDH-A facilitates tumor progression are poorly understood.

We studied 2 isogenic cell lines (67NR and 4T1) originating from the same mammary tumor (21). Both cell lines generate orthotopic breast tumors with different growth and metastatic profiles (21): 67NR cells form primary tumors but no metastases, whereas 4T1 cells generate tumors that rapidly complete all steps leading to macroscopic nodules in lungs within 6 to 8 days of orthotopic implantation. In this study, we show that these cell lines and their corresponding orthotopic tumors have different metabolic profiles as well.

Significant differences in the gene expression pattern of 4T1 and 67NR cells have been described (22, 24, 36), and these differences contribute to the distinct metabolic and phenotypic behaviors of 4T1 and 67NR cells and tumors. A substantial number of highly expressed genes in 4T1 cells/tumors are associated with cell adhesion, migration, angiogenesis, extracellular matrix modification, cytoskeleton function, cell proliferation, apoptosis, survival, inflammation, immune response, and cellular metabolism. 4T1 cells also displayed elevated levels of *Gadd45*, *Pfkfb3*, *Vegfc*, *Flt1*; some of these genes are known to be regulated by hypoxia and glucose deprivation. This gene expression profile suggests that 4T1 cells are in a stress-related state, with high metabolic requirements that are inadequately supplied by the vasculature leading to hypoxia and glucose deprivation.

Our additional analysis of published data (22, 36) identified several other important modulators of tumor metabolism. Carbonic anhydrase isoform-12 (CA12) in 4T1 cells is expressed 6.7-fold above that in 67NR cells. CA12 is a transmembrane enzyme that maintains normal intracellular pH and is known to be upregulated by hypoxia-inducible factor 1. Furthermore, a 2.3-fold elevation of MYC expression was observed in 4T1 cells compared

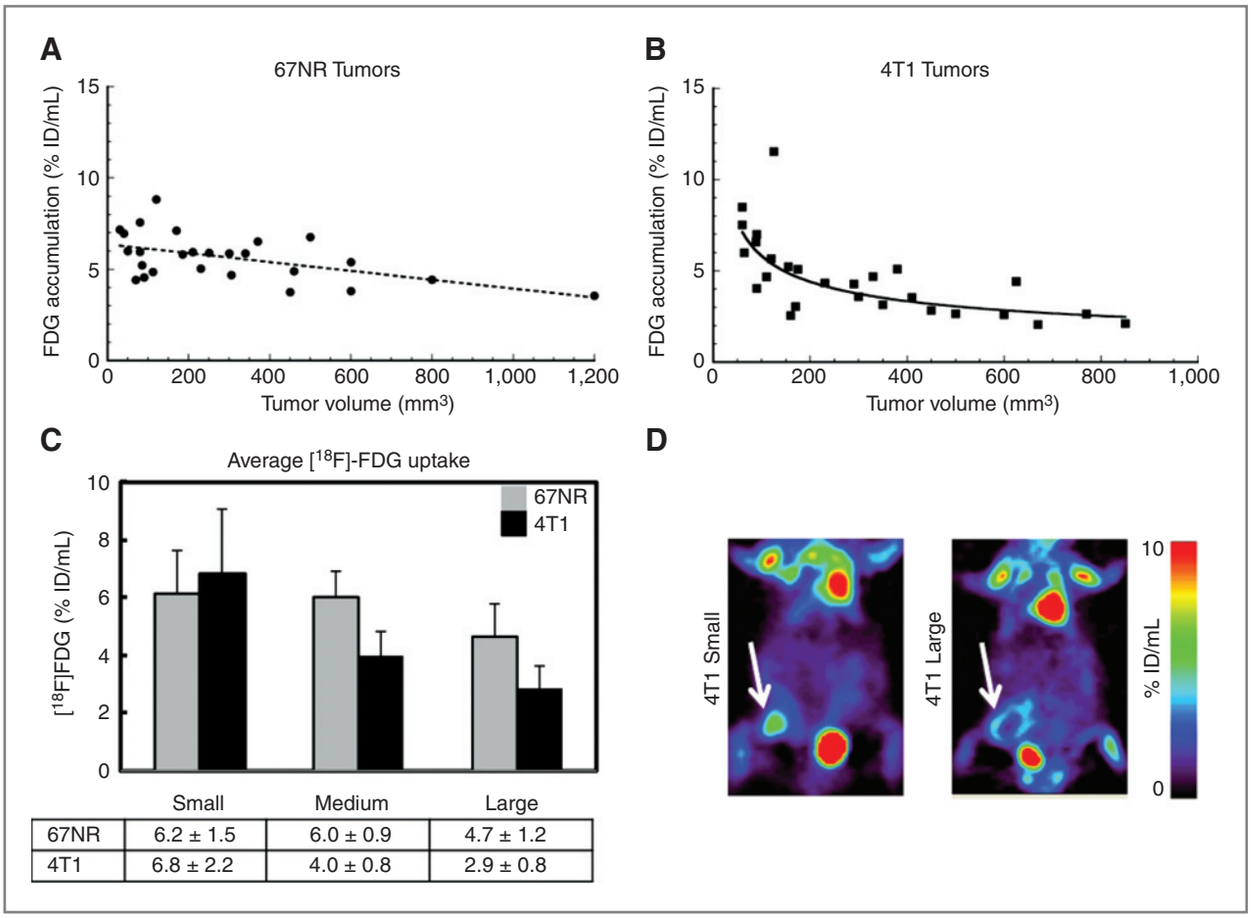

	Small	Medium	Large
67NR	6.2 ± 1.5	6.0 ± 0.9	4.7 ± 1.2
4T1	6.8 ± 2.2	4.0 ± 0.8	2.9 ± 0.8

Figure 4. FDG-PET measurements of [^{18}F]FDG accumulation in orthotopic 67NR and 4T1 breast tumors during tumor growth. [^{18}F]FDG accumulation in (A) 67NR tumors (solid circles, dashed line) and in (B) 4T1 tumors (solid squares, solid line) plotted versus tumor volume. C, average [^{18}F]FDG accumulation at 3 different tumor volumes (small, <150 mm^3; medium, 150–400 mm^3; and large, >400 mm^3). Values are the mean ± SD. D, representative [^{18}F]FDG microPET images of tumor-bearing mice; small and large 4T1 orthotopic tumors are visualized (white arrows). High radioactivity is seen in the cervical brown fat, heart, and bladder. Values are color coded to a range of values (%ID/mL).

with nonmetastatic 67NR cells (22). This raises the interesting possibility of a link between glucose and glutamine metabolism in these cells because Myc induces mitochondrial biogenesis in proliferating cells (37), stimulates mitochondrial glutamine metabolism (38), and upregulates *LDH-A* (39). In addition to data from gene expression analyses, comprehensive proteomics profiling across these cell lines has been conducted (40). The majority of the detected changes in protein expression are associated with metabolism-related proteins (>40%) including the expression of LDH-A (40).

A recently completed metabolomic analysis of the same cells using liquid chromatography/tandem mass spectroscopy confirmed the above observations (41). The metastatic capacity of 4T1 cells was shown to be associated with altered glycolysis, pentose phosphate pathway, and fatty acid synthesis, as well as decreased reduced glutathione/oxidized glutathione redox pool. In addition, 4T1 cells have shown enrichment of TCA cycle intermediates (citrate, isocitrate, and malate; ref. 41), which correlates with a 3.2-fold higher expression of malic enzyme in 4T1 cells (36). These data coincide with a recent study (42) showing that breast cancer cells with the potential to form brain metastases may use aerobic glycolysis coupled to the TCA cycle and oxidative phosphorylation to generate energy for cell growth. However, it is unclear whether the increase in TCA cycle activity is driven primarily by glucose or by glutamine metabolism, and additional studies will be required to answer this question.

The metabolism of both glucose and glutamine involves LDH. LDH is a tetrameric enzyme, containing 2 major subunits (A and B) coded by 2 different genes (*LDH-A* and *LDH-B*), which may form 5 isozymes (43). All 5 isozymes can catalyze the forward and backward conversion of pyruvate and lactate. LDH-A (LDH-5, M-LDH, or A4) kinetically favors the conversion of pyruvate to lactate whereas LDH-B (LDH-1, H-LDH, or B4) predominantly converts lactate to pyruvate, which will be further oxidized through the TCA cycle (44). The LDH-A and LDH-B subunits and their ratio are very important in the formation

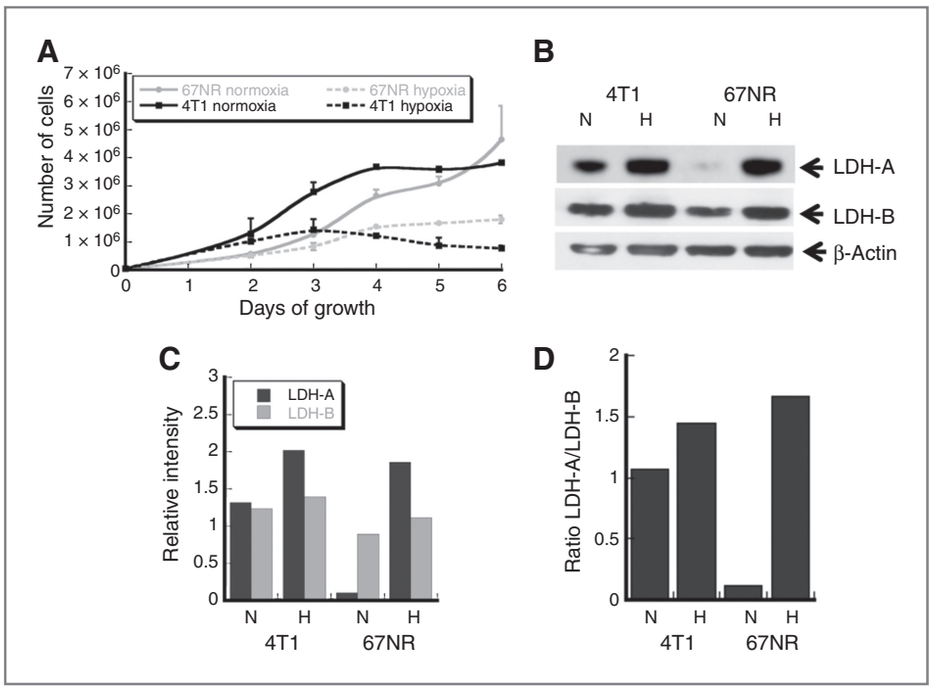

Figure 5. The effect of hypoxia on the cell growth and LDH-A expression. A, growth profiles of 67NR cells and 4T1 cells under normoxic (N, 21%) and hypoxic (H, 1%) conditions. B, immunoblot analysis of LDH-A and LDH-B subunits from 67NR and 4T1 cells exposed to normoxia and hypoxia for 24 hours. C, the β-actin–normalized intensity of LDH-A and LDH-B levels in cells under normoxic and hypoxic conditions. D, the ratio of β-actin–normalized LDH-A and LDH-B expression under normoxic and hypoxic conditions.

and function of the tetrameric enzyme, and the subunit composition impacts on the kinetics and the direction of the LDH-regulated reaction.

We found nearly equal levels of LDH-A and LDH-B expression in 4T1 cells using immunoblot analysis. The LDH-A/LDH-B ratio was 1.0 and 1.4 in 4T1 cells under normoxia and hypoxia, respectively. In 67NR cells the corresponding LDH-A/LDH-B ratio variation was much greater under normoxia and hypoxia, ranging from 0.11 to 1.66, respectively. The LDH isozymes of 4T1 and 67NR cells have the capacity to catalyze pyruvate–lactate reactions in both directions, with a tendency toward lactate formation under hypoxic conditions. Moreover, these results (reflecting a change in the LDH-A/LDH-B tetrameric enzyme ratio) are consistent with the oxygen consumption experiments, where high mitochondrial TCA cycle activity was observed in 4T1 cells and with the *in vivo* MRSI experiments showing high lactate and early development of necrosis in small 4T1 tumors. The hypoxia-induced change in the LDH-A/LDH-B tetrameric enzyme ratio of 67NR cells was more dramatic and consistent with the appearance of lactate in medium- and large-size 67NR tumors. Under hypoxia, 67NR cells significantly upregulate LDH-A and change the composition of the LDH enzymatic complex with the preference toward lactate formation (44).

The higher LDH-A expression in 4T1 cells than in 67NR cells under normal oxygen conditions is reflected in higher LDH enzymatic activity, higher lactate production, greater generation of hydrogen ions, and a greater consumption of glucose by 4T1 cells. In contrast with a traditional Warburg phenotype, 4T1 cells consume oxygen significantly faster than 67NR cells, showing high mitochondrial respiration in these metastatic-prone cancer cells. In the last several years, a number of publications have shown that oncogenes, such as *c-Myc* (37) and mutant *H-Ras* (45), increase mitochondrial metabolism which correlated with metastatic potential. Importantly, active oxidative phosphorylation could be very essential for the *in vivo* growth of highly glycolytic tumors, which could be a step to recycle secreted lactate to fuel mitochondrial activity (46) or be an adaptation to other metabolic stress (47, 48). In addition, the anchorage-independent growth phenotype, which is an important signature of metastatic tumors, is also associated with the activated mitochondrial biogenesis (49).

Several noninvasive imaging techniques can be used for the assessment of tumor metabolism. MRI/MRS provides a unique ability to noninvasively obtain structural as well as metabolic information from soft tissues. [^{18}F]FDG-PET is primarily used in tumor diagnosis to stage the extent of disease and to monitor the response to therapy (50); the magnitude of FDG uptake has also been shown to reflect, in part, the rate of glycolysis (50). The capability of MRSI to noninvasively obtain metabolic information is a valuable asset in the metabolic profiling of tumors and can provide molecular signatures of specific biological processes in discreet anatomic structures using natural metabolites and stable (nonradioactive) isotopes (^{13}C, ^{15}N, etc.). Using SelMQC transfer in combination with CSI for *in vivo* lactate detection, we have shown striking differences and changes in tumor lactate levels during orthotopic 67NR and 4T1 breast tumors growth. A 10-fold higher level of lactate was measured in small (<150 mm^3) 4T1 tumors than in small 67NR tumors (Fig. 3). Lung metastases are known to develop early (~6–8 days after orthotopic implantation

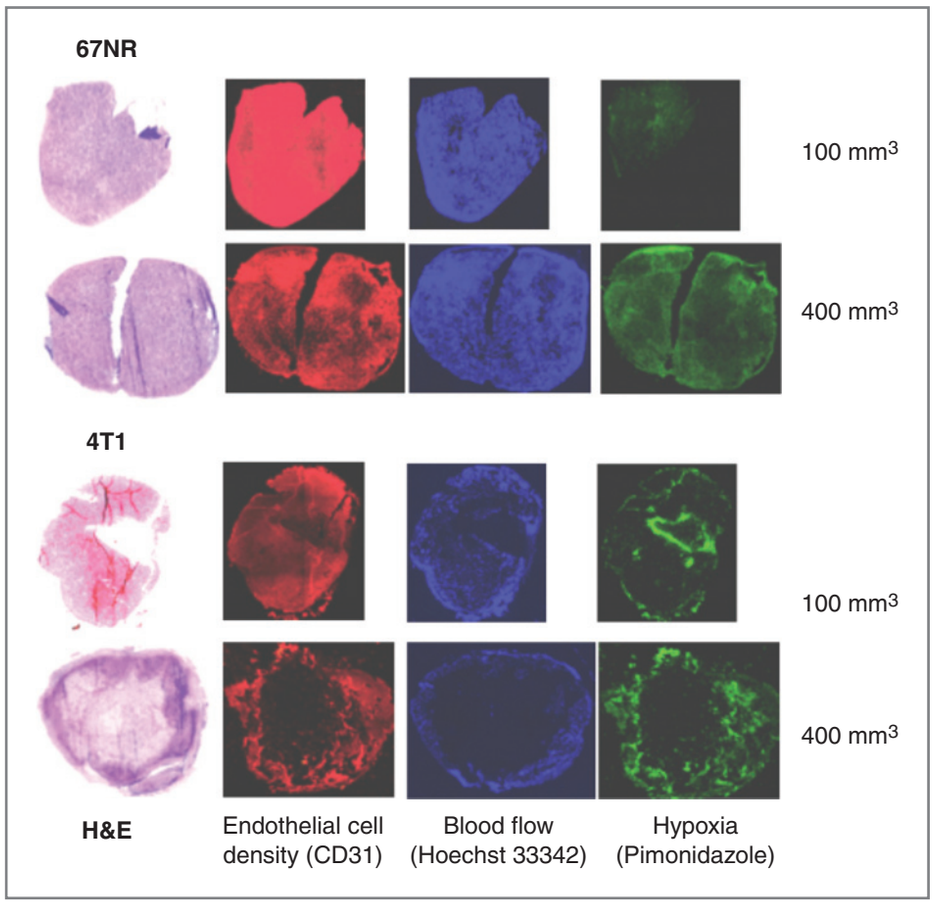

Figure 6. Immunohistochemical staining of 67NR and 4T1 tumors. Histology (H&E), endothelial cell density (CD31, red), blood flow (Hoechst 33342, blue), and hypoxia (Pimonidazole, green) are compared. Small 67NR tumors showed no necrosis, a uniform endothelial cell density and blood flow, and no hypoxia. Medium-size 67NR tumors showed some pimonidazole staining. This small 4T1 tumor shows some central necrosis, a decrease in endothelial cell density, and blood flow, with a corresponding zone of hypoxia surrounding the necrotic zone. These observations were amplified in medium-size 4T1 tumors.

of 4T1 cells; Supplementary Fig. S4; ref. 21) and at approximately the same time that 4T1 tumor lactate levels are very high (11.0 ± 1.5 mmol/L, 8 days after implantation; Fig. 3D). The correspondence of high lactate levels in small 4T1 tumors and concurrent development of lung metastases is of particular interest and suggests that high levels of lactate may be associated with the initiation of metastases.

Differences in lactate production and microenvironment acidity have been previously shown to differentiate metastatic and nonmetastatic human xenografts (51, 52). The high lactate concentration (~10 mmol/L; Fig. 3D) measured in small 4T1 tumors, concurrent with the development of lung metastases (days 6–8; Supplementary Fig. S4), is consistent with clinical studies (4, 6) where high lactate levels (with median concentrations >8 mmol/L) were associated with the subsequent development of metastases (4).

In comparison to tumor lactate levels, there were only small changes in [^{18}F]FDG accumulation during 4T1 and 67NR tumor growth. At the time metastases were developing from small orthotopic 4T1 tumors, there was only a 1.1-fold difference in [^{18}F]FDG accumulation between 4T1 and 67NR tumors. In contrast, there was a 10-fold difference in lactate levels in the same tumors at the time when there was little or no tumor necrosis. The subsequent decline in lactate concentration and [^{18}F]FDG accumulation during 4T1 tumor growth may reflect the effects of tumor necrosis. Because tumor lactate concentration and [^{18}F]FDG accumulation are likely to be related in a glycolytic phenotype, we compared the ratio of tumor lactate concentration and tumor [^{18}F]FDG accumulation, sequentially during tumor growth. Despite a fair amount of scatter, 67NR and 4T1 tumors showed marked differences in their lactate/FDG ratio profiles when the tumors were small (Supplementary Fig. S5) whereas both tumors approached a similar plateau ratio (1.0–1.1 mmol/L/%ID/mL) as they increased in size.

Cellular oxygen consumption is one of the determinants of intracellular oxygen levels (53). Under conditions of high oxygen demand, cells can become hypoxic due to high oxygen consumption (54). This is reflected in the metabolic profiles observed for small 4T1 and 67NR tumors and is very similar to those observed in the cell culture experiments. It suggests that the *in vitro* cell culture environment may better reflect the *in vivo* environment of small tumors. Thus, *in vitro* cell cultures may be better models for small well-perfused tumors prior to the development of significant ischemia, hypoxia, and necrosis. In culture, 4T1 cells produce lactate and consume significantly more glucose and oxygen than 67NR cells. The appearance of necrotic

zones, even in small 4T1 tumors at the time early metastases are developing, is likely to reflect an oxygen requirement for efficient 4T1 cell metabolism and may contribute to hypoxia-induced cell death in these tumors. Moreover, the significant necrosis observed in all enlarging 4T1 tumors (Supplementary Fig. S3) is associated with lower levels of lactate production in medium- and large-size 4T1 tumors. The intensity of the pimonidazole staining was also significantly higher in all 4T1 samples than in 67NR tumors. Less-intense hypoxia staining was observed only in the larger 67NR tumors and is consistent with the gradual increase and plateau of lactate concentration in medium and large sizes 67NR tumors.

This study presents several important findings: (i) The expression of LDH-A and production of lactate in 4T1 breast cancer cells and small orthotopic tumors are higher than in isogenic 67NR cells and tumors; (ii) Changes in LDH-A level under hypoxic conditions could explain the formation of lactate in larger 67NR tumors; (iii) MRSI was considerably better than [^{18}F]FDG-PET in identifying significant differences in the metabolic phenotype of small 4T1 tumors (high lactate production and high glucose utilization) than in 67NR tumors, and these differences were most prominent during early tumor growth when 4T1 metastases were developing; and (iv) Lactate-MRSI has a greater dynamic range than [^{18}F]FDG-PET and may be a more sensitive measure with which to evaluate the aggressive potential of primary breast tumors.

Disclosure of Potential Conflicts of Interest

No potential conflicts of interest were disclosed.

Acknowledgments

We thank Mihaela Lupu for excellent technical assistance, Dr. Sean Carlin for providing some material and valuable discussions, Drs. Pat Zanzonico and Peter Smith-Jones for providing data for partial volume corrections, and Dr. Steven Larson for help and generous support.

Grant Support

This work was supported in part by funds: BC060114, CA098505, CA115675, CA86438, CA94060, U24CA83084, and DOD W81XWH-09-1-0042 (S.B. Thakur).

The costs of publication of this article were defrayed in part by the payment of page charges. This article must therefore be hereby marked *advertisement* in accordance with 18 U.S.C. Section 1734 solely to indicate this fact.

Received February 11, 2011; revised July 21, 2011; accepted July 27, 2011; published OnlineFirst August 15, 2011.

References

1. Gatenby RA, Gillies RJ. A microenvironmental model of carcinogenesis. Nat Rev Cancer 2008;8:56–61.
2. Gatenby RA, Gillies RJ. Why do cancers have high aerobic glycolysis? Nat Rev Cancer 2004;4:891–9.
3. Warburg O. On respiratory impairment in cancer cells. Science 1956;124:269–70.
4. Walenta S, Mueller-Klieser WF. Lactate: mirror and motor of tumor malignancy. Semin Radiat Oncol 2004;14:267–74.
5. Walenta S, Wetterling M, Lehrke M, Schwickert G, Sundfor K, Rofstad EK, et al. High lactate levels predict likelihood of metastases, tumor recurrence, and restricted patient survival in human cervical cancers. Cancer Res 2000;60:916–21.
6. Brizel DM, Schroeder T, Scher RL, Walenta S, Clough RW, Dewhirst MW, et al. Elevated tumor lactate concentrations predict for an increased risk of metastases in head-and-neck cancer. Int J Radiat Oncol Biol Phys 2001;51:349–53.
7. Walenta S, Chau TV, Schroeder T, Lehr HA, Kunz-Schughart LA, Fuerst A, et al. Metabolic classification of human rectal adenocarcinomas: a novel guideline for clinical oncologists? J Cancer Res Clin Oncol 2003;129:321–6.
8. Wise DR, Thompson CB. Glutamine addiction: a new therapeutic target in cancer. Trends Biochem Sci 2010;35:427–33.
9. Vander Heiden MG, Cantley LC, Thompson CB. Understanding the Warburg effect: the metabolic requirements of cell proliferation. Science 2009;324:1029–33.
10. Fantin VR, St-Pierre J, Leder P. Attenuation of LDH-A expression uncovers a link between glycolysis, mitochondrial physiology, and tumor maintenance. Cancer Cell 2006;9:425–34.
11. Koukourakis MI, Giatromanolaki A, Sivridis E, Bougioukas G, Didilis V, Gatter KC, et al. Lactate dehydrogenase-5 (LDH-5) overexpression in non-small-cell lung cancer tissues is linked to tumour hypoxia, angiogenic factor production and poor prognosis. Br J Cancer 2003;89:877–85.
12. Koukourakis MI, Giatromanolaki A, Simopoulos C, Polychronidis A, Sivridis E. Lactate dehydrogenase 5 (LDH5) relates to up-regulated hypoxia inducible factor pathway and metastasis in colorectal cancer. Clin Exp Metastasis 2005;22:25–30.
13. Koukourakis MI, Giatromanolaki A, Sivridis E, Gatter KC, Harris AL; Tumour Angiogenesis Research Group. Lactate dehydrogenase 5 expression in operable colorectal cancer: strong association with survival and activated vascular endothelial growth factor pathway–a report of the Tumour Angiogenesis Research Group. J Clin Oncol 2006;24:4301–8.
14. Ryberg M, Nielsen D, Osterlind K, Andersen PK, Skovsgaard T, Dombernowsky P. Predictors of central nervous system metastasis in patients with metastatic breast cancer. A competing risk analysis of 579 patients treated with epirubicin-based chemotherapy. Breast Cancer Res Treat 2005;91:217–25.
15. Koukourakis MI, Giatromanolaki A, Sivridis E, Gatter KC, Trarbach T, Folprecht G, et al. Prognostic and predictive role of lactate dehydrogenase 5 (LDH5) expression in colorectal cancer patients treated with PTK787/ZK 222584 (Vatalanib) anti-angiogenic therapy. Clin Cancer Res 2011;17:4892–900.
16. Le A, Cooper CR, Gouw AM, Dinavahi R, Maitra A, Deck LM, et al. Inhibition of lactate dehydrogenase A induces oxidative stress and inhibits tumor progression. Proc Natl Acad Sci U S A 2010;107:2037–42.
17. Seth P, Grant A, Tang J, Vinogradov E, Wang X, Lenkinski R, et al. On-target inhibition of tumor fermentative glycolysis as visualized by hyperpolarized pyruvate. Neoplasia 2011;13:60–71.
18. Xie H, Valera VA, Merino MJ, Amato AM, Signoretti S, Linehan WM, et al. LDH-A inhibition, a therapeutic strategy for treatment of hereditary leiomyomatosis and renal cell cancer. Mol Cancer Ther 2009;8:626–35.
19. Nevins JR, Potti A. Mining gene expression profiles: expression signatures as cancer phenotypes. Nat Rev Genet 2007;8:601–9.
20. Gupta GP, Massague J. Cancer metastasis: building a framework. Cell 2006;127:679–95.
21. Aslakson CJ, Miller FR. Selective events in the metastatic process defined by analysis of the sequential dissemination of subpopulations of a mouse mammary tumor. Cancer Res 1992;52:1399–405.
22. Tao K, Fang M, Alroy J, Sahagian GG. Imagable 4T1 model for the study of late stage breast cancer. BMC Cancer 2008;8:228.

23. Heppner GH, Miller FR, Shekhar PM. Nontransgenic models of breast cancer. Breast Cancer Res 2000;2:331–4.
24. Eckhardt BL, Parker BS, van Laar RK, Restall CM, Natoli AL, Tavaria MD, et al. Genomic analysis of a spontaneous model of breast cancer metastasis to bone reveals a role for the extracellular matrix. Mol Cancer Res 2005;3:1–13.
25. Firth JD, Ebert BL, Ratcliffe PJ. Hypoxic regulation of lactate dehydrogenase A. Interaction between hypoxia-inducible factor 1 and cAMP response elements. J Biol Chem 1995;270:21021–7.
26. Ebert BL, Gleadle JM, O'Rourke JF, Bartlett SM, Poulton J, Ratcliffe PJ. Isoenzyme-specific regulation of genes involved in energy metabolism by hypoxia: similarities with the regulation of erythropoietin. Biochem J 1996;313:809–14.
27. Kroemer G, Pouyssegur J. Tumor cell metabolism: cancer's Achilles' heel. Cancer Cell 2008;13:472–82.
28. Urano M, Chen Y, Humm J, Koutcher JA, Zanzonico P, Ling C. Measurements of tumor tissue oxygen tension using a time-resolved luminescence-based optical oxylite probe: comparison with a paired survival assay. Radiat Res 2002;158:167–73.
29. He Q, Shungu DC, van Zijl PC, Bhujwalla ZM, Glickson JD. Single-scan *in vivo* lactate editing with complete lipid and water suppression by selective multiple-quantum-coherence transfer (Sel-MQC) with application to tumors. J Magn Reson B 1995;106:203–11.
30. Muruganandham M, Koutcher JA, Pizzorno G, He Q. *In vivo* tumor lactate relaxation measurements by selective multiple-quantum-coherence (Sel-MQC) transfer. Magn Reson Med 2004;52:902–6.
31. Yaligar J, Thakur SB, Bokacheva L, Carlin S, Thaler HT, Rizwan A, et al. Lactate MRSI and DCE MRI as surrogate markers of prostate tumor aggressiveness. NMR Biomed 2011. Epub 2011 May 25.
32. Danielsen ER, Michaelis T, Ross BD. Three methods of calibration in quantitative proton MR spectroscopy. J Magn Reson B 1995;106: 287–91.
33. Moroz M, Kochetkov T, Cai S, Wu J, Shamis M, Nair J, et al. Imaging colon cancer response following treatment with AZD1152: a preclinical analysis of [18F]fluoro-2-deoxyglucose and 3′-deoxy-3′-[18F]fluorothymidine imaging. Clin Cancer Res 2011;17:1099–110.
34. Carlin S, Khan N, Ku T, Longo VA, Larson SM, Smith-Jones PM. Molecular targeting of carbonic anhydrase IX in mice with hypoxic HT29 colorectal tumor xenografts. PLoS One 2010;5:e10857.
35. Granchi C, Bertini S, Macchia M, Minutolo F. Inhibitors of lactate dehydrogenase isoforms and their therapeutic potentials. Curr Med Chem 2010;17:672–97.
36. Yang J, Mani SA, Donaher JL, Ramaswamy S, Itzykson RA, Come C, et al. Twist, a master regulator of morphogenesis, plays an essential role in tumor metastasis. Cell 2004;117:927–39.
37. Li F, Wang Y, Zeller KI, Potter JJ, Wonsey DR, O'Donnell KA, et al. Myc stimulates nuclearly encoded mitochondrial genes and mitochondrial biogenesis. Mol Cell Biol 2005;25:6225–34.
38. Wise DR, DeBerardinis RJ, Mancuso A, Sayed N, Zhang XY, Pfeiffer HK, et al. Myc regulates a transcriptional program that stimulates mitochondrial glutaminolysis and leads to glutamine addiction. Proc Natl Acad Sci U S A 2008;105:18782–7.
39. Shim H, Dolde C, Lewis BC, Wu CS, Dang G, Jungmann RA, et al. c-Myc transactivation of LDH-A: implications for tumor metabolism and growth. Proc Natl Acad Sci U S A 1997;94:6658–63.
40. Ho J, Kong JW, Choong LY, Loh MC, Toy W, Chong PK, et al. Novel breast cancer metastasis-associated proteins. J Proteome Res 2009;8:583–94.
41. Lu X, Bennet B, Mu E, Rabinowitz J, Kang Y. Metabolomic changes accompanying transformation and acquisition of metastatic potential in a syngeneic mouse mammary tumor model. J Biol Chem 2010; 285:9317–21.
42. Chen EI, Hewel J, Krueger JS, Tiraby C, Weber MR, Kralli A, et al. Adaptation of energy metabolism in breast cancer brain metastases. Cancer Res 2007;67:1472–86.
43. Everse J, Kaplan NO. Lactate dehydrogenases: structure and function. Adv Enzymol Relat Areas Mol Biol 1973;37:61–133.
44. Stambaugh R, Post D. Substrate and product inhibition of rabbit muscle lactic dehydrogenase heart (H4) and muscle (M4) isozymes. J Biol Chem 1966;241:1462–7.
45. Telang S, Lane AN, Nelson KK, Arumugam S, Chesney J. The oncoprotein H-RasV12 increases mitochondrial metabolism. Mol Cancer 2007;6:77.
46. Sonveaux P, Vegran F, Schroeder T, Wergin MC, Verrax J, Rabbani ZN, et al. Targeting lactate-fueled respiration selectively kills hypoxic tumor cells in mice. J Clin Invest 2008;118:3930–42.
47. Chen V, Shtivelman E. CC3/TIP30 regulates metabolic adaptation of tumor cells to glucose limitation. Cell Cycle 2010;9:4941–53.
48. Wellen KE, Thompson CB. Cellular metabolic stress: considering how cells respond to nutrient excess. Mol Cell 2010;40:323–32.
49. Mori S, Chang JT, Andrechek ER, Matsumura N, Baba T, Yao G, et al. Anchorage-independent cell growth signature identifies tumors with metastatic potential. Oncogene 2009;28:2796–805.
50. Mankoff DA, Eary JF, Link JM, Muzi M, Rajendran JG, Spence AM, et al. Tumor-specific positron emission tomography imaging in patients: [18F] fluorodeoxyglucose and beyond. Clin Cancer Res 2007;13:3460–9.
51. Schornack PA, Gillies RJ. Contributions of cell metabolism and H+ diffusion to the acidic pH of tumors. Neoplasia 2003;5:135–45.
52. Jordan BF, Black K, Robey IF, Runquist M, Powis G, Gillies RJ. Metabolite changes in HT-29 xenograft tumors following HIF-1alpha inhibition with PX-478 as studied by MR spectroscopy *in vivo* and *ex vivo*. NMR Biomed 2005;18:430–9.
53. Hagen T, Taylor CT, Lam F, Moncada S. Redistribution of intracellular oxygen in hypoxia by nitric oxide: effect on HIF1alpha. Science 2003;302:1975–8.
54. Aragones J, Schneider M, Van Geyte K, Fraisl P, Dresselaers T, Mazzone M, et al. Deficiency or inhibition of oxygen sensor Phd1 induces hypoxia tolerance by reprogramming basal metabolism. Nat Genet 2008;40:170–80.